# First complete set of spin 3/2 nuclear scattering analyzing powers

P. D. Cathers, E. E. Bartosz, M. W. Cooper, N. Curtis, N. Keeley, K. W. Kemper, F. Maréchal, E. G. Myers, and B. G. Schmidt
*Department of Physics, Florida State University, Tallahassee, Florida 32306*

K. Rusek
*Department of Nuclear Reactions, The Andrzej Sołtan Institute for Nuclear Studies, Hoża 69, 00-681 Warsaw, Poland*

V. Hnizdo*
*Department of Physics, University of Witwatersrand, Johannesburg 2050, South Africa*
(Received 26 June 2000; published 26 April 2001)

The first complete set of analyzing powers for any nuclear spin $\frac{3}{2}$ beam is reported. Analyzing powers and elastic cross section are presented for $^4$He($^7\vec{\text{Li}}$,$^7$Li)$^4$He at the two center of mass energies of 11.5 and 16.5 MeV. An optical model analysis of these data shows the need for spin-orbit and second rank tensor potentials in addition to real and imaginary central potentials. The inclusion of triton transfer improves the description of the large angle elastic scattering cross section but has little impact on the calculated analyzing powers. The description of the third rank analyzing powers $iT_{31}$ and $iT_{33}$ is poor at small angles, and no combination of potentials including a large third rank potential is able to describe them. No real evidence for the presence of a third rank potential is found.

DOI: 10.1103/PhysRevC.63.064601 PACS number(s): 24.70.+s, 25.70.Bc

## I. INTRODUCTION

The pioneering studies of polarized $^{6,7}$Li scattering by the Hamburg-Heidelberg-Marburg group found two remarkable results. The first was that the measured vector analyzing power was of opposite sign for $^6$Li and $^7$Li elastic scattering [1]. The second was that the elastic second rank tensor analyzing power for $^7$Li scattering was much larger than that for $^6$Li scattering [2,3]. Both sets of data were taken at energies where the scattering was of the Fresnel type so that semiclassical models could be applied to them. The second rank tensor analyzing power results provided clear evidence for scattering from the nonspherical part of the $^7$Li mass distribution. Later coupled-channels calculations showed that the vector analyzing powers arise from virtual excitation coupling between the projectile states rather than from a spin-orbit potential.

With the availability of higher-energy polarized Li beams, it became possible to obtain analyzing power data in the Fraunhofer scattering regime. Measurements of cross sections and analyzing powers for the elastic scattering of $^{6,7}$Li+$^{12}$C at about 20 MeV [3,4] and $^{6,7}$Li+$^{26}$Mg at 44 MeV [5,6] were obtained. While the second rank tensor analyzing powers for $^7$Li were still considerably larger than those for $^6$Li there was no clear contrast between the vector analyzing powers of the two isotopes, with both exhibiting considerable oscillatory structure. However, the vector and second rank tensor analyzing powers could still be understood in terms of channel couplings to the excited states and the deformed shape of $^7$Li. The vector analyzing powers were not as well described as in the Fresnel scattering regime.

In addition to their different shapes, the other major difference between the Li isotopes is their nuclear spins. For $^6$Li the ground state spin $J=1$, whereas for $^7$Li, $J=3/2$. This has important consequences for the spin observables that can be measured for the two isotopes. For nuclei of spin $J=1$ only analyzing powers up to and including the second rank tensor exist, whereas for nuclei of spin $J=3/2$ third rank tensor analyzing powers may be measured in addition to the vector and second rank tensor. Previously, the only third rank analyzing power that has been measured for $^7$Li scattering is $^TT_{30}$, for both the the Fresnel [7] and Fraunhofer [5] scattering regimes. In both cases, $^TT_{30}$ was found to be very small (essentially zero for the Fraunhofer scattering) and virtually structureless.

While $^TT_{30}$ could be well described for the Fresnel data (44 MeV $^7$Li+$^{120}$Sn), to date no calculation has been able to fit this analyzing power for the Fraunhofer data (44 MeV $^7$Li+$^{26}$Mg). Tungate *et al.* [7] found that they were able to obtain a good description of $^TT_{30}$ for the $^7$Li +$^{120}$Sn elastic scattering without the need for a third rank tensor potential. Coupled-channels calculations [5,8] for the $^7$Li+$^{26}$Mg elastic scattering produced large, highly oscillatory $^TT_{30}$ angular distributions, in contrast to the measured values.

The motivation for the current work is threefold. First, by measuring a complete set of third rank analyzing powers we wished to establish whether *all* the third rank analyzing powers are small, as $^TT_{30}$ is a ''composite'' analyzing power formed by combining $iT_{31}$ and $iT_{33}$. Thus, it may be small due to cancellation of these two analyzing powers. Coupled with this, we also wished to establish whether the third rank analyzing powers remain small for a light target such as $^4$He

*Present address: National Institute for Occupational Safety and Health, Morgantown, WV 26505.

 

and at a higher relative bombarding energy than the previous measurements. Secondly, we wished to investigate the question as to whether a third rank tensor potential was necessary to describe third rank analyzing powers. Using simple $\alpha$-$t$ cluster folding arguments, Mukhopadhyay *et al.* [9] postulated the existence of a third rank tensor potential of second derivative Woods-Saxon form. However, as mentioned above, Tungate *et al.* [7] found no evidence of the need for such a potential to describe ${}^{T}T_{30}$ for 44 MeV $^{7}$Li+$^{120}$Sn elastic scattering. Again, we wished to establish whether this finding still holds for lighter targets and in the Fraunhofer scattering regime. Finally, there is the question of the physical origin of the third rank analyzing powers; what process or processes actually generates them? We leave this question to a future investigation employing continuum-discretized-coupled-channels (CDCC) calculations.

The present work reports the first complete set of elastic scattering analyzing powers measured for a spin 3/2 projectile. Complete sets of analyzing powers including the full third rank were measured at the two center-of-mass bombarding energies of 11.5 and 16.5 MeV for the system $^{7}$Li $+^{4}$He. The target $^{4}$He was chosen because it has no low-lying excited state so that the observed analyzing powers should arise solely from the $^{7}$Li projectile. Also, a complete set of $^{6}$Li+$^{4}$He analyzing powers has been recently published [10] so that a comparison of the two data sets provides a direct measurement of the role played by the structure of the two nuclei. The present results, when combined with recently published $^{6}$He+$^{4}$He [11] and $^{6}$Li+$^{4}$He [10] data, provide data sets that can test models of scattering by loosely bound nuclei.

The new data set is analyzed in this work in terms of phenomenological optical potentials. A search was made for evidence of the presence of a third rank tensor potential in the $^{7}$Li+$^{4}$He interaction. The possible role of triton exchange in this scattering was also investigated. The applicability of the shape effect relations [12–14], which allow the second rank tensor analyzing powers $T_{20}$, $T_{21}$, and $T_{22}$ to be obtained from ${}^{T}T_{20}$, was also investigated.

## II. EXPERIMENTAL PROCEDURE

The Florida State University (FSU) optically pumped polarized lithium ion source (OPPLIS) [15] was used to produce a $^{7}$Li beam preferentially in one of the $^{7}$Li magnetic substates $m_I=\frac{3}{2}$, $\frac{1}{2}$, $-\frac{1}{2}$, and $-\frac{3}{2}$, referred to as state $N_m$. The data acquisition system cycled the polarization state of the beam automatically through the unpolarized state and each of the polarized states $N_m$ as required, spending approximatively three minutes in each state. After ionization and charge exchange in a cesium charge exchange cell, the beam passed through the magnetic field of a Wien filter to properly orient the spin quantization axis. It was then accelerated by the FSU Super FN Tandem accelerator to an energy of 34 MeV. The scattering chambers consisted of an 85 cm diameter evacuated chamber followed by a helium-filled chamber at 380 Torr. The 34 MeV beam was slowed down to 31.5 MeV in the helium target volume by passing through a Havar foil, which isolated the helium gas from the evacuated 85 cm chamber, and 26 cm of gas to the center of the helium-filled chamber. For the 16.5 MeV c.m. analyzing power measurements, the FSU Superconducting Linear Accelerator provided additional acceleration to 47.6 MeV, which was reduced to 45.5 MeV within the helium target volume. All the analyzing power data reported here were taken in the helium-filled chamber, while the beam polarization on target was measured in the 85 cm scattering chamber.

Two $\Delta E$-$E$ silicon surface barrier telescopes, placed symmetrically on each side of the beam, were arranged to rotate about the center of the helium-filled chamber. The collimation system on each telescope subtended a polar angular width of 0.8°. The angular calibration of the detectors was established by normalizing the relative yields to the absolute cross section angular distribution reported by Bingham *et al.* [16] for $\alpha+^{6}$Li at $E_{\mathrm{c.m.}}=11.1$ MeV. An unpolarized $^{6}$Li beam from the Cs sputter source was used for this angular calibration. The $\Delta E$ thickness was chosen such that the scattered $^{7}$Li and recoil $^{4}$He nuclei could be distinguished at all angles, allowing measurements simultaneously at two c.m. scattering angles, one forward and one backward, for each detector angle setting.

The beam polarizations were calculated using the equations

$$t_{10}=\sqrt{\frac{9}{5}}\left[(n_{3/2}-n_{-3/2})+\frac{1}{3}(n_{1/2}-n_{-1/2})\right],$$

$$t_{20}=(n_{3/2}+n_{-3/2})-(n_{1/2}+n_{-1/2}),$$

$$t_{30}=\sqrt{\frac{9}{5}}\left[\frac{1}{3}(n_{3/2}-n_{-3/2})-(n_{1/2}-n_{-1/2})\right], \qquad (1)$$

where the fractional populations $n_m$ of the substates $m_I$, normalized by $\Sigma_m n_m=1$, were measured at the source by means of laser induced fluorescence (LIF) and were measured on target using the $p(^{7}\mathrm{Li},\alpha)\alpha$ reaction at 0° [7] in the 85 cm chamber. The beam polarization was measured approximately every two hours with this detector during the data acquisition. Typical beam polarization values were $t_{10}=0.54\pm0.02$, $t_{20}=0.60\pm0.03$, and $t_{30}=0.55\pm0.03$. The lithium beam polarizations produced by OPPLIS have been found over several years of operation to be stable to within $\pm5\%$ when the optimum laser power level for the optical pumping is maintained. This stability was observed during the present work.

The spin axis orientations and the equations used to measure the analyzing powers in this work are presented here, with attention to the appropriate sign changes required for use with the recoil nuclei data. The Madison frame has the $\hat{z}$ axis parallel to the projectile momentum $\hat{k}_i$ and the $\hat{y}$ axis given by $\hat{k}_i\times\hat{k}_f$ where $\hat{k}_f$ is the direction of the ejectile momentum. In this frame, the direction of the spin axis on target is defined by the angles $\beta$ and $\phi$, with $\beta$ measured from the $\hat{z}$ axis to the spin axis and $\phi$ measured from the $\hat{y}$ axis to the projection of the spin axis onto the $x$-$y$ plane. The cross section $\sigma_{\mathrm{pol}}$ measured for a spin $\frac{3}{2}$ polarized beam is expanded in the Madison frame as

$$\sigma_{\rm pol}=\sigma_{\rm unp}\Big[1+\sqrt{2}\sin\beta\cos\phi t_{10}iT_{11}+\frac{1}{2}(3\cos^2\beta-1)t_{20}T_{20}+\sqrt{3/2}\sin 2\beta\sin\phi t_{20}T_{21}-\sqrt{3/2}\sin^2\beta\cos 2\phi t_{20}T_{22}+\frac{1}{2}\sqrt{3}\sin\beta(5\cos^2\beta-1)\cos\phi t_{30}iT_{31}+\sqrt{15/8}\sin\beta\sin 2\beta\sin 2\phi t_{30}iT_{32}-\frac{1}{2}\sqrt{5}\sin^3\beta\cos 3\phi t_{30}iT_{33}\Big]. \quad (2)$$

When the polarization axis is set parallel to the beam momentum ($\beta=0°$), Eq. (2) reduces to

$$\frac{\sigma_{\rm pol}}{\sigma_{\rm unp}}-1=L-1=t_{20}T_{20}, \quad (3)$$

where $\sigma_{\rm pol}$ and $\sigma_{\rm unp}$ refer to the observed cross sections resulting from the use of polarized and unpolarized beams, respectively and $L$ is defined as $\sigma_{\rm pol}/\sigma_{unp}$. This equation also holds for the right detector observations, labeled $R$. This equation does not change sign upon measurement of a recoil nucleus. The beam was cycled through the unpolarized state and the $N_{3/2}$ state to create a large $t_{20}$.

With a spin axis orientation defined as $\beta=135°$ and $\phi=270°$, the analyzing power $T_{21}$ of a scattered nucleus can be determined using the relation

$$L-R=\sqrt{6}t_{20}T_{21}. \quad (4)$$

The value of $L-R$ changes sign upon measurement of a recoil nucleus. At the same orientation, the tensor analyzing power ${}^{T}T_{20}$ of a scattered nucleus can be determined using the relation

$$L+R-2=-t_{20}{}^{T}T_{20}. \quad (5)$$

It should be noted that this equation is given incorrectly in Ref. [17], the minus sign in front of $t_{20}$ being omitted there. This equation does not change sign upon measurement of a recoil nucleus. The beam was cycled through the unpolarized state and the $N_{3/2}$ state to create a large $t_{20}$.

A spin axis orientation on target of $\beta=90°$ and $\phi=30°$ yields

$$L-R=\sqrt{6}t_{10}iT_{11}-\frac{3}{2}t_{30}iT_{31}. \quad (6)$$

The value of $L-R$ changes sign upon measurement of a recoil nucleus. The beam was cycled through the unpolarized state and the $N_{1/2}$ state to create a large $t_{30}$.

A spin axis orientation on target of $\beta=54.7°$ and $\phi=45°$ yields

$$L+R-2=2.1t_{30}iT_{32}. \quad (7)$$

This equation does not change sign upon measurement of a recoil nucleus. The beam was cycled through the unpolarized state and the $N_{1/2}$ state to create a large $t_{30}$.

The transverse frame [19] has the $\hat{y}$ axis parallel to the projectile momentum $\hat{k}_i$ and the $\hat{z}$ axis given by $\hat{k}_i\times\hat{k}_f$ where $\hat{k}_f$ is the direction of the ejectile momentum. The angle $\psi$ is measured from the $\hat{z}$ axis to the spin axis and $\rho$ is measured from the $\hat{x}$ axis to the projection of the spin axis onto the $x$-$y$ plane, the reaction plane. The analyzing powers expressed in the transverse frame are denoted by a left superscript $T$, and the polarized cross section $\sigma_{\rm pol}$ is written

$$\sigma_{\rm pol}=\sigma_{\rm unp}\Big[1+\cos\psi t_{10}{}^{T}T_{10}+\frac{1}{2}(3\cos^2\psi-1)t_{20}{}^{T}T_{20}-\sqrt{3/8}\sin^2\psi t_{20}({}^{T}T_{2,-2}e^{2i\rho}+{}^{T}T_{22}e^{-2i\rho})+\frac{1}{2}(5\cos^3\psi-3\cos\psi)t_{30}{}^{T}T_{30}+\sqrt{15/8}\sin^2\psi\cos\psi t_{30}({}^{T}T_{3,-2}e^{2i\rho}+{}^{T}T_{32}e^{-2i\rho})\Big]. \quad (8)$$

Orienting the spin quantization axis in the direction normal to the scattering plane at $\psi=180°$, i.e., ''down,'' the set of equations

$$t_{10}^{N_{3/2}}=-\frac{9}{5{}^{T}T_{10}}\left[\frac{1}{\sum_i L_i}[2L_{3/2}+4/3L_{1/2}+2/3L_{-1/2}]-1\right],$$

$$t_{20}^{N_{3/2}}=+\frac{1}{{}^{T}T_{20}}\left[\frac{1}{\sum_i L_i}[L_{3/2}-L_{1/2}-L_{-1/2}+L_{-3/2}]\right],$$

$$t_{30}^{N_{3/2}}=-\frac{3}{5{}^{T}T_{30}}\left[\frac{1}{\sum_i L_i}[4/3L_{3/2}+2L_{-1/2}+2/3L_{-3/2}]-1\right] \quad (9)$$

holds, where $L_m$ denotes the polarized to unpolarized cross section ratio seen by the left detector with the beam in the $N_m$ polarization state. The sum is over $i=3/2,1/2,-1/2,-3/2$. The equation for $t_{30}$ is given incorrectly in Refs. [17, 18], which have $L_{1/2}$ in place of $L_{-1/2}$. Upon measurement of a recoil nucleus, the second rank equation does not change sign, but the odd ranks do. Note that for the right detector ($R$), the spin axis orientation may be expressed as $\psi=0°$ and the odd ranks of Eq. (9) will contain an additional overall negative sign. At the same orientation, normal to the scattering plane at $\psi=180°$, i.e., ''down,'' the second ranks are isolated using only one polarization state and the ''off'' state,

$$\frac{1}{2}(L+R-2)=t_{20}{}^{T}T_{20}. \quad (10)$$

This equation does not change sign upon measurement of a recoil nucleus. The beam was cycled through the unpolarized state and each of the $N_m$ states.

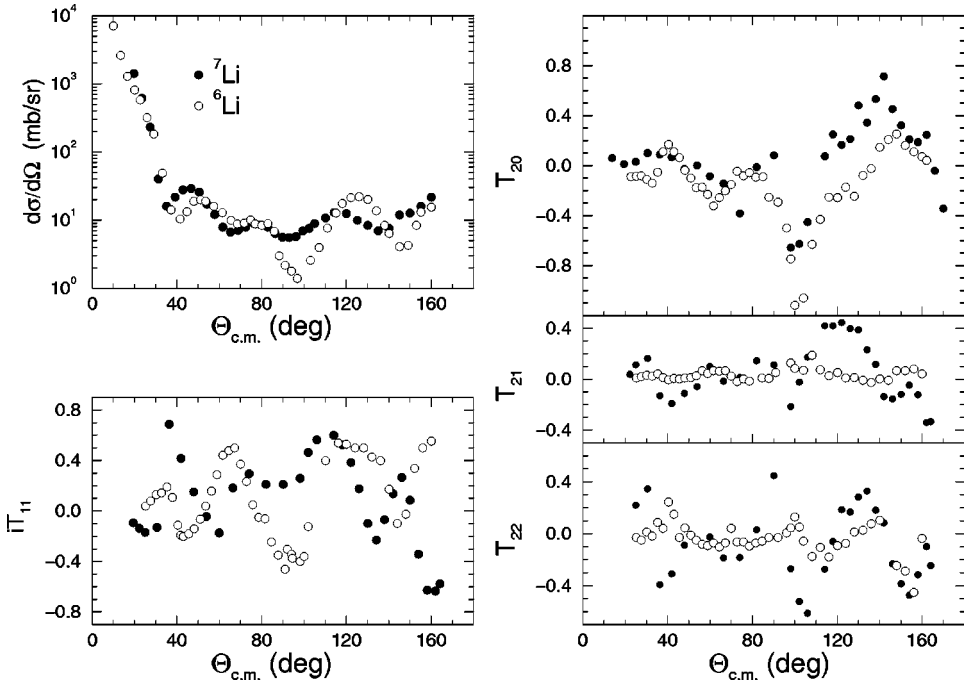


FIG. 1. Cross section, vector analyzing power $iT_{11}$, and second rank tensor analyzing powers $T_{20}$, $T_{21}$, and $T_{22}$ for the $^6$Li+$^4$He elastic scattering at 11.1 MeV c.m. (open circles) and for the present $^7$Li+$^4$He elastic scattering at 11.5 MeV c.m. (solid circles). The $^6$Li data are from Ref. [10].

The remaining analyzing powers may be found through the interframe relations

$$T_{22} = -\sqrt{\frac{2}{3}}\left[{}^{T}T_{20} + \frac{1}{2}T_{20}\right], \tag{11}$$

$$iT_{33} = -\sqrt{\frac{4}{5}}\left(\sqrt{\frac{3}{4}}iT_{31} + {}^{T}T_{30}\right). \tag{12}$$

For the unpolarized $^7$Li($^4$He,$^4$He)$^7$Li differential cross section measurements, the spherical deflector of OPPLIS was removed and replaced by a radio frequency helium source which ionized the atoms to the $^4$He$^+$ state. The helium ions, negatively charged after charge exchange, were accelerated by the FSU Super FN Tandem accelerator to energies of 18 and 26 MeV, corresponding to center of mass energies of 11.5 and 16.5 MeV, respectively. The beam then scattered off a 100 $\mu$g/cm$^2$ $^7$Li target enriched to 99%, evaporated onto a Formvar backing, and placed in the 85 cm scattering chamber. Two $\Delta E$-$E$ silicon surface barrier telescopes were mounted symmetrically in the chamber on either side of the beam axis to allow identification of the scattered $\alpha$ particles. One telescope was kept fixed, serving as a monitor of beam intensity and target conditions while the other detector telescope was moved through the different angle settings of the distribution. Both the scattered $\alpha$ and the recoil $^7$Li nuclei were detected simultaneously so that two angles in the distribution were measured at once. The Havar foil and helium filled chamber were replaced by a beam stop so that proper beam current integration could be achieved during the angular distribution runs. The data at 11.5 MeV c.m. were normalized to that of Bingham *et al.* [16] to obtain the product $N d\Omega$ of the target thickness times the detector solid angle, needed to establish the absolute cross section for the 16.5 MeV c.m. scattering. The absolute error in the 11.5 MeV c.m. cross sections reported in Ref. [16] was 5%. The absolute error in the 16.5 MeV data is 8% and is based on the measurements of $N d\Omega$ on four separate occasions.

## III. ANALYSIS AND RESULTS

The importance of comparing $^6$Li and $^7$Li analyzing power measurements was dramatically demonstrated with early vector analyzing power results for $^{6,7}$Li+$^{58}$Ni elastic scattering [1–3]. Tungate *et al.* [1] showed that, in the Fresnel regime, the elastic scattering vector analyzing power was positive for $^6$Li+$^{58}$Ni and negative for $^7$Li+$^{58}$Ni. However, folding model calculations that included a realistic spin-orbit potential predicted positive vector analyzing powers for both projectiles. In addition, subsequent work found that the magnitude of the second rank tensor analyzing power ${}^{T}T_{20}$ was small ($<0.03$) for $^6$Li+$^{58}$Ni, but considerably larger ($\sim -0.15$) for $^7$Li+$^{58}$Ni [2].

Previous elastic scattering analyzing power measurements for the system $^6$Li+$^4$He reported by Green *et al.* [10] at a c.m. energy of 11.1 MeV may be compared to the present $^7$Li+$^4$He data. The $^6$Li+$^4$He data were well described by a phenomenological optical model analysis that required an explicit but relatively weak spin-orbit potential, and an angular momentum dependent imaginary potential. An explicit second rank tensor potential was found to be relatively unimportant.

Figure 1 displays the present 11.5 MeV c.m. $^7$Li data along with the 11.1 MeV c.m. $^6$Li data of Green *et al.* [10]. In contrast to what was found in the Fresnel scattering regime there is no clear difference between the vector analyzing powers for the two Li isotopes, $iT_{11}$ being large and exhibiting considerable oscillatory structure for both $^6$Li and $^7$Li. The main difference between the two data sets is in the second rank analyzing power $T_{21}$, which is very close to

zero for the $^6$Li scattering, but large for the $^7$Li scattering. $T_{22}$ is much larger for $^7$Li than for $^6$Li but the difference is not as dramatic as for $T_{21}$, especially at large angles.

The two nuclei are both characterized by a low breakup threshold ($\sim$1.48 MeV for $^6$Li and $\sim$2.47 MeV for $^7$Li) but have very different ground state quadrupole moments. The nucleus $^6$Li is almost spherical ($Q_s=-0.09$ $e$ fm$^2$) whereas $^7$Li is highly deformed ($Q_s=-4.00$ $e$ fm$^2$). Comparing the two present data sets shows that these structure differences also dominate several features of the elastic scattering data in the Fraunhofer scattering regime. However, it also shows that some features are similar in the two data sets in this predominantly nuclear scattering regime.

### A. $^7$Li shape effect

The large spectroscopic quadrupole moment of $^7$Li has been shown to play a major role in the scattering of polarized $^7$Li. When the $^7$Li beam is aligned, its quadrupole moment is also aligned and in a semiclassical picture presents a shape different from that of an unpolarized beam. During the first $^7$Li tensor polarized scattering experiments trends in the data showed a definite relationship between the second rank tensor analyzing powers. By assuming that the object being scattered, i.e., $^7$Li has an oblate shape, Tungate *et al.* [12] and Moroz *et al.* [2] derived the shape effect relations.

The shape effect relations which connect the second rank analyzing powers are given by

$$T_{20}=-\frac{1}{2}(1-3\cos\theta)^T T_{20}(\theta),$$

$$T_{21}=-\sqrt{\frac{3}{2}}\sin\theta^T T_{20}(\theta),$$

$$T_{22}=-\sqrt{\frac{3}{8}}(1+\cos\theta)^T T_{20}(\theta), \tag{13}$$

where $\theta$ is the scattering angle. These relations were originally developed for scattering near the Coulomb barrier where semi-classical models could be used. However, Gomez *et al.*, with a quantum-mechanical derivation, extended their application to all energies where the nuclear interaction is important by invoking the concept of tidal symmetry [13]. Subsequently, Ott *et al.* determined the regions where this symmetry is not broken and therefore should apply [14]. These regions correspond to those where the isocentrifugal approximation, assumed by Gomez *et al.*, is valid. Ott *et al.* derive an isocentrifugal parameter $d$ which is small ($<0.2$) for scatterings which satisfy this criterion. The shape effect relations apply for scattering in the Fresnel regime, which involves heavy targets with low $^7$Li bombarding energies, as $d$ is always small in these cases. This regime is characterized by smooth angular distributions for both cross section and analyzing powers. On the other hand, scatterings in the Fraunhofer regime, which involves light targets and high beam energies, have oscillatory cross section angular distributions and do not follow the shape effect relations as well as scatterings in the Fresnel regime. Ott *et al.* demonstrate that elastic scattering in the Fraunhofer regime can follow the shape relations quite closely, provided that the isocentrifugal approximation is valid and $d$ is small. This was found to be the case for the 44 MeV $^7$Li+$^{26}$Mg elastic scattering, which is in the Fraunhofer regime but for which the shape effect relations still hold to a reasonable approximation.

The present scattering data are in the Fraunhofer regime, as expected for a very light target such as $^4$He, and have large ($>0.4$) values of $d$. Therefore, we do not expect these data to be very well described by the shape effect relations but it is important nevertheless to test this expectation. The results are shown in Fig. 2 for the $^7$Li+$^4$He elastic scattering at the two c.m. energies of 11.5 and 16.5 MeV. The data for each second rank tensor analyzing power are given by the solid circles, while the solid lines are calculated using Eqs. (13). Although the shape relations give values which do at times follow the data, this is probably merely fortuitous. The lower energy 11.5 MeV data clearly follows these relations better than the 16.5 MeV data even though the 11.5 MeV second rank tensor analyzing powers are larger and more oscillatory than those at 16.5 MeV. This result is to be expected from the arguments of Ott *et al.*, as the lower energy has a smaller value of $d$.

### B. Optical model calculations

The goal of the optical model analysis described here is to determine the form of the potentials required to describe the measured cross sections and analyzing powers, including whether a third rank tensor potential is required to describe the third rank analyzing powers.

The central imaginary potential was modified to account for the possibility that the large cross section found in scattering from light targets at backward angles results from the inability of the system to absorb a larger angular momentum. This modification, known as $J$ dependence, has been shown to simulate the strong virtual channel coupling found in $^6$Li scattering [20,21] when combined with phenomenological Woods-Saxon central potentials.

The calculations were carried out using the optical model code HERMES [22], which allows the calculation of third rank analyzing powers. Since this code had not been extensively used to calculate third rank analyzing powers, numerous checks of this part of the code were carried out. An error in the calculation of the third rank analyzing power $iT_{31}$ was found and traced back to a paper by Cook and Philpott [23] which lays out the matrix element summations used in HERMES for a spin 3/2 system. The correct equation for $iT_{31}$, which was inserted in HERMES, is

$$\sigma iT_{31}=\sqrt{\frac{1}{5}}Im[(AB^*+CD^*+EF^*+GH^*) -\sqrt{3}(BC^*+FG^*)]. \tag{14}$$

The only change between Eq. (14) and the original equation (6f) in Ref. [23] is to replace the last $E$ in the equation with an $F$.

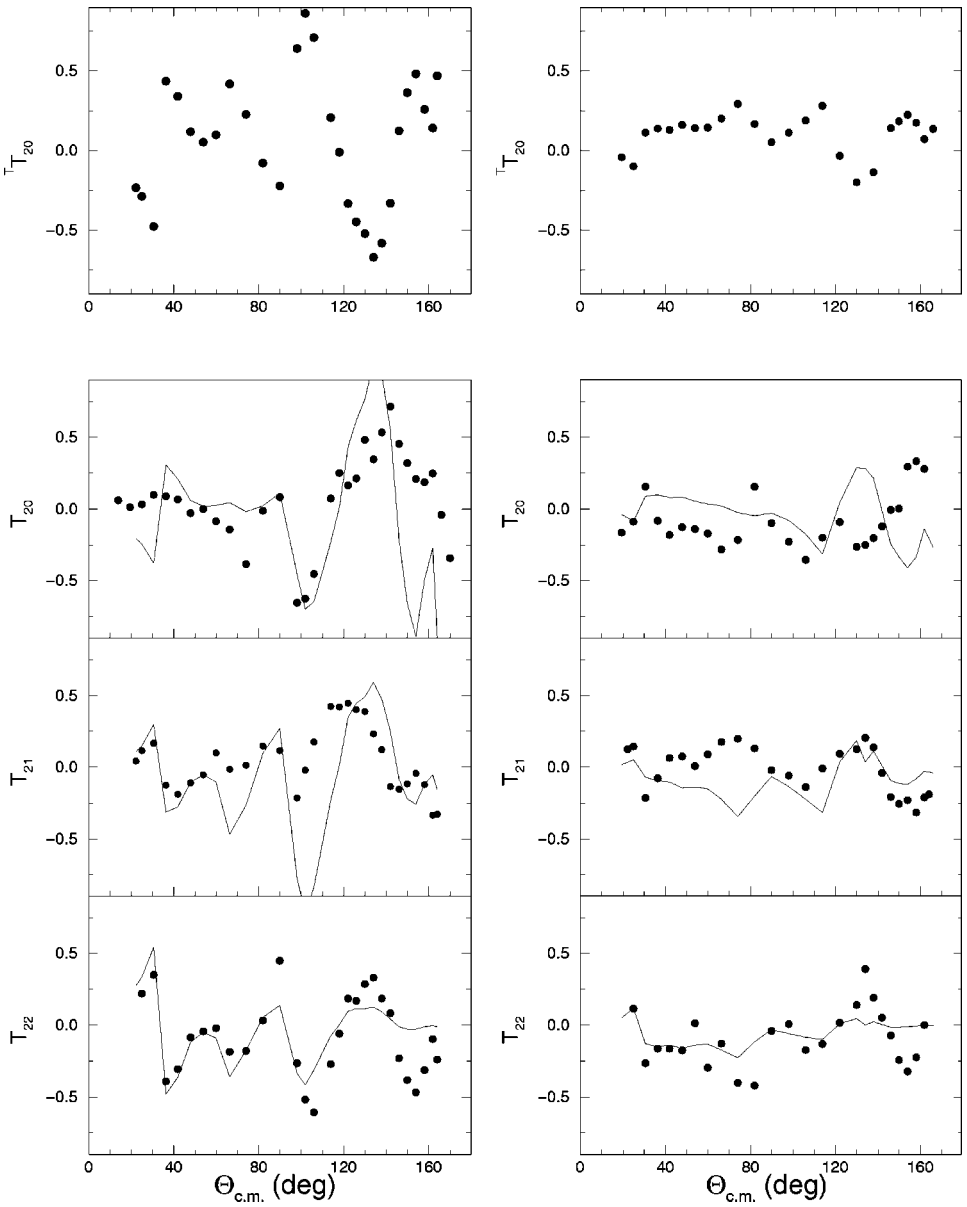


FIG. 2. Second rank analyzing powers measured for the $^{7}$Li $+^{4}$He elastic scattering at 11.5 MeV c.m. (left) and 16.5 MeV c.m. (right). The solid lines show the shape effect relations calculated using Eqs. (13).

The potentials used in the calculations are real and imaginary Woods-Saxon central potentials, real and imaginary spin-orbit potentials, and real rank-2 and -3 tensor potentials. The forms of the potentials used in HERMES are outlined by Cook [22], with the *J*-dependence modification of the imaginary central potential given by Trcka *et al.* [20,21]. These potentials all utilize the volume Woods-Saxon radial form given by

$$f_x(r)=\left[1+\exp\left(\frac{(r-R_x)}{a_x}\right)\right]^{-1}, \tag{15}$$

where $a_x$ is the diffuseness and the radius $R_x$ uses the convention $R_x=r_xA_T^{1/3}$, where $A_T$ is the mass of the target nucleus and $r_x$ is the radius parameter used in HERMES. The real and imaginary central potentials are given by the Woods-Saxon potential form

$$V(r)=-V_0f_x(r). \tag{16}$$

The imaginary part invokes an angular momentum dependent absorption and contains an extra factor $f(J)=[1+e^{(J-J_c)/\Delta J}]^{-1}$. The parameters $J_c$ and $\Delta J$ are the cutoff and diffuseness angular momentum parameters [20,21]. In HERMES, the real and imaginary spin-orbit potentials have the Thomas form given by

$$V_{\mathrm{SO}}(r)=\left(\frac{\hbar}{m_\pi c}\right)^2\frac{V_{\mathrm{SO}}}{r}\frac{d}{dr}f_x(r), \tag{17}$$

where $(\hbar/m_\pi c)$ is the pion Compton wavelength, and is multiplied by $(\vec{l}\cdot\vec{s})$ for the full potential. A Raynal tensor potential [24] of the form

$$V_{T_2}(r)=-6\sqrt{3}V_{T_2}\frac{d^2}{dr^2}f_x(r) \tag{18}$$

TABLE I. Optical model parameters used in the HERMES and FRESCO calculations. The Coulomb radius $R_c$ was 3.31 fm. Set 1(3) describes the 16.5(11.5) MeV data using the optical model with $J$ dependence. Set 2(4) is used for the 16.5(11.5) MeV calculations that include the transfer contribution. The radius parameters $r_x$ are given as $R_x = r_x A_T^{1/3}$. The potential numbers in brackets are values in FRESCO that give the same elastic scattering description as HERMES. Potential depths are in MeV, radius, and diffuseness in fm.

| Set | | 1 | 2 | 3 | 4 |
|---|---|---|---|---|---|
| Central | $V$ | 100.2 | 153.2 | 120.2 | 136.2 |
| Real | $r_R$ | 1.71 | 2.2 | 1.71 | 2.2 |
| | $a_r$ | 0.65 | 0.44 | 0.65 | 0.58 |
| Central | $W$ | 20.5 | 15.6 | 12.5 | 12.4 |
| Imaginary | $r_W$ | 3.09 | 2.2 | 3.09 | 2.2 |
| | $a_W$ | 0.65 | 0.44 | 0.65 | 0.58 |
| Spin orbit | $V_{LS}$ | 1.0 | 7.4(3.7) | 1.0 | 7.4(3.7) |
| | $r_{LS}$ | 2.5 | 2.2 | 2.5 | 2.2 |
| | $a_{LS}$ | 0.65 | 0.44 | 0.65 | 0.58 |
| Spin orbit | $W_{LS}$ | 2.8 | | 2.8 | |
| Imaginary | $r_{W_{LS}}$ | 2.5 | | 2.5 | |
| | $a_{W_{LS}}$ | 0.65 | | 0.65 | |
| Tensor | $V_{T_2}$ | −3.87 | −1.47(−8.3) | −3.87 | −2.57(−10.0) |
| | $r_{T_2}$ | 1.5 | 2.2 | 1.5 | 2.2 |
| | $a_{T_2}$ | 0.45 | 0.44 | 0.55 | 0.58 |
| Third rank | $V_{T_3}$ | −3.67 | | −3.67 | |
| | $r_{T_3}$ | 1.5 | | 1.3 | |
| | $a_{T_3}$ | 0.45 | | 0.45 | |
| $J$ dependence | $J_C$ | 3.8 | | 3.8 | |
| | $\Delta J$ | 1.2 | | 1.2 | |

is used when second rank tensor potentials are included. Finally, for the third rank potential, the Irshad and Robson tensor potential [25] is used and its form is given by

$$V_{T_3}(r) = -V_{T_3} r^2 \frac{d^2}{dr^2} f_x(r). \tag{19}$$

This form was chosen for the third rank potential following the work of Mukhopadhyay *et al.* [9]. Using a simple $\alpha$-$t$ cluster folding picture of $^7$Li they derived a potential for $^7$Li elastic scattering consisting of central, spin-orbit, and second and third rank tensor potentials. The central and second rank tensor potentials arose from the central $\alpha$-target and $t$-target potentials used in the folding procedure, whereas the spin-orbit and third rank tensor potentials were produced by the $t$-target spin-orbit potential. The central form factor was found to be of Woods-Saxon shape, while the spin-orbit form factor was of the usual Woods-Saxon derivative shape. Both the second and third rank tensor potentials were of second derivative Woods-Saxon shape. Based on these arguments, we confined our search for a third rank tensor potential to one of second derivative form.

The parameter sets 1 and 3 in Table I were obtained by starting with the $^6$Li+$^4$He parameters of Green *et al.* [10]. Owing to the large number of data points and the size of the parameter space involved, merely minimizing $\chi^2$ in order to obtain the best fit was found to be inadequate. Consequently, a series of grid searches was carried out and the results plotted using a semiautomated procedure. The quality of the resultant fits was then assessed subjectively. This process led to the best simultaneous fits to the cross section and analyzing power data that we were able to obtain.

The grid searches were carried out in the following manner. The real central potential depth was varied from 80 to 110 MeV in steps of 10 MeV and the imaginary potential depth was varied from 15 to 25 MeV in steps of 2.5 MeV. The real spin-orbit potential depth was varied from 5 to 10 MeV in steps of 2.5 MeV while the tensor potential depth was varied from 2 to 5 MeV in 1 MeV steps. The $J$-dependence parameter $J_C$ was varied from 2.5 to 4.5 in steps of 1 while the diffuseness $\Delta J$ was varied from 0.8 to 1.6 in steps of 0.4. Also, the radii were varied from 1 to 3 fm in 1 fm steps while the diffuseness was tried at 0.45, 0.65, and 0.85 fm.

This grid search mainly established the parameters for the central potentials and $J$-dependence terms, and gave only an idea of the values for the rest of the parameters. The central potentials were ''fine tuned'' by considering just the cross section, and then the spin-dependent potentials (spin-orbit, second, and third rank tensor) were added to the calculations. The values of the parameters for these potentials were fine-tuned by considering their effects on the analyzing powers. These spin-dependent potentials are much weaker than the central potential so their effect on the cross section was expected to be small. However, we ensured that the cross section was not adversely affected while the spin-dependent potentials were being varied. The optical potential parameters were established for the 16.5 MeV data first. These parameters were then used as a starting point for the 11.5 MeV searches. The final parameter values for the best descriptions of the 16.5 MeV and 11.5 MeV data are given by sets 1 and 3 in Table I, respectively.

All the optical model calculations included $J$-dependent imaginary central potentials. If the $J$ dependence was not included, the calculations were found to be insensitive to the presence of the spin-dependent potentials (spin-orbit, second, and third rank tensor). The basic (real + $J$-dependent imaginary central potentials) calculation generated analyzing powers of all ranks, as expected since the $J$-dependence factor represents channel coupling to the excited states of $^7$Li. However, the predicted values of $T_{21}$ and the third rank analyzing powers were considerably smaller than the data at both energies.

In contrast to what was found by Green *et al.* [10] for the 11.1 MeV $^6$Li+$^4$He case we were unable to obtain a good description of the vector and second rank tensor analyzing powers at either energy by just including a spin-orbit potential in addition to the $J$-dependent central potential. The inclusion of an imaginary spin-orbit potential was found to improve the fit at both energies, although it was more important at 16.5 MeV. For the best description of the data, a second rank tensor potential was essential. The dashed curves in Figs. 3 and 4 show the results of calculations using

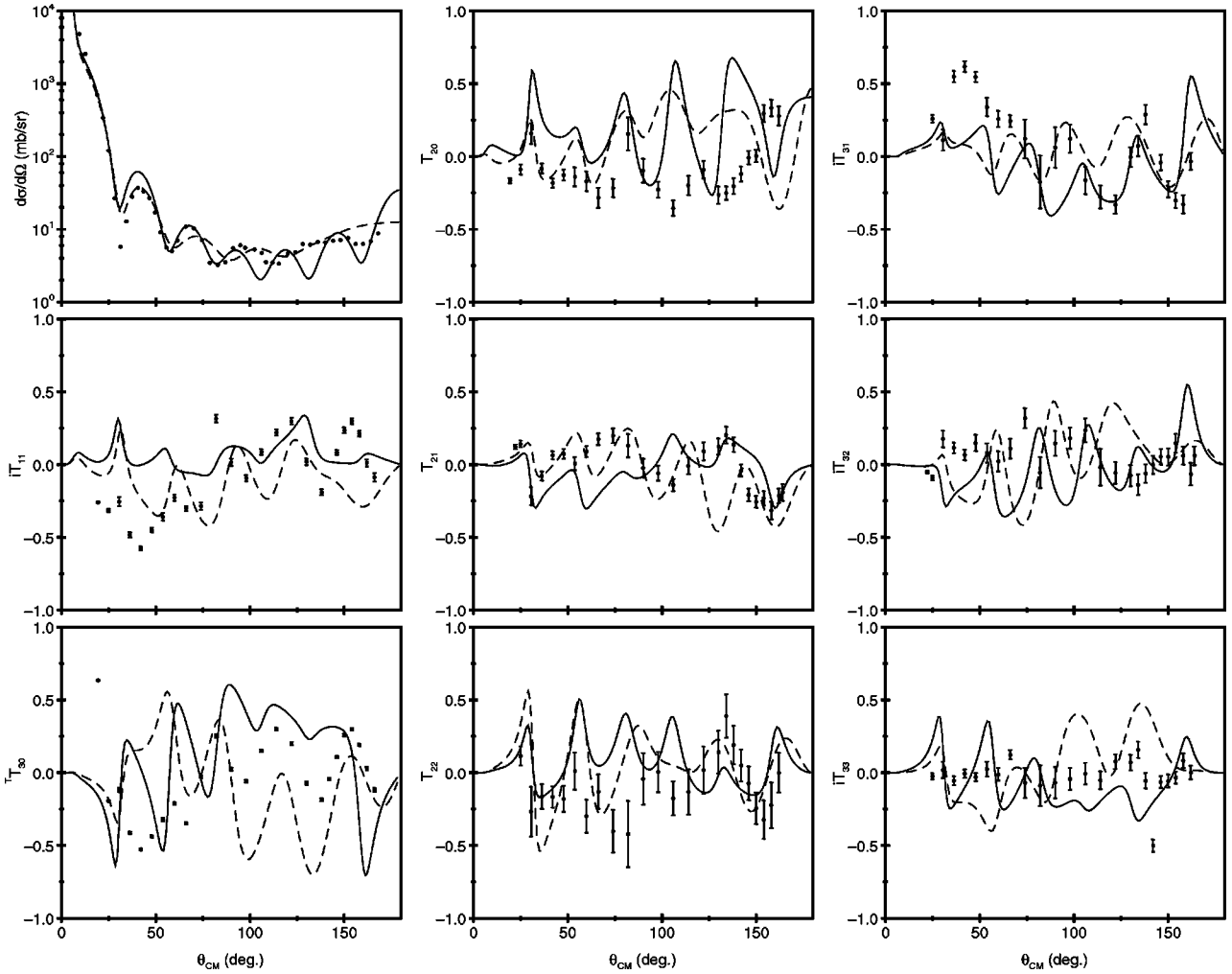


FIG. 3. Cross section and analyzing power angular distributions measured for the $^7$Li+$^4$He elastic scattering at a c.m. energy of 16.5 MeV. The full calculation using the optical model parameter set 1 in Table I is shown by the solid lines. The dashed lines show the full calculation without use of the third rank potential.

sets 1 and 3 of Table I, but including the *J*-dependent imaginary potential and spin-orbit and second rank tensor potentials only.

The full curves in Figs. 3 and 4 denote the results of calculations including a third rank tensor potential, of the Irshad and Robson form [25]. At 16.5 MeV there is little case for arguing the need for a third rank tensor potential of this form. Its inclusion cannot be said to improve the overall fit to the data, which is poor in general. By contrast, at 11.5 MeV there is a definite improvement in the overall description of the data when the third rank tensor potential is included, as Fig. 4 shows. The general quality of the fit at 11.5 MeV is considerably better than that at 16.5 MeV.

### C. FRDWBA calculations

The sizable measured elastic scattering cross section at back angles ($\theta_{\text{c.m.}} \geqslant 120°$) may be indicative of a large contribution from triton transfer, and this possibility was investigated by FRDWBA calculations using the code FRESCO [26]. In this transfer, the triton from the $^7$Li projectile is picked up by the $^4$He target to form another $^7$Li. As the target $^4$He is heavier than the triton, the newly formed $^7$Li travels backwards in the c.m., and is experimentally inseparable from the backscattered $^7$Li beam nucleus. Initially, HERMES with no *J* dependence was used to determine the optical model parameters needed to produce the distorting potentials for the transfer calculations [20,21,27]. The *J*-dependent potential had been introduced [20,21] to reproduce the larger than expected experimental cross section observed for $\alpha$ particle and heavy-ion scattering at large angles. In this analysis it is assumed that the large value of the cross section observed at back angles comes from the transfer reaction. The optical model calculations concentrated on describing the elastic cross section data for angles less than 90°, which should have very little transfer contribution. An optical model calculation with FRESCO was then performed to make sure the two codes agreed. Then, these optical model parameters were used in the FRDWBA transfer calculations to determine the importance of the triton transfer.

Starting with the values of Bingham *et al.* [16], the optical potential parameters for the 16.5 MeV case were set first. A second rank tensor potential, which Bingham *et al.* did not

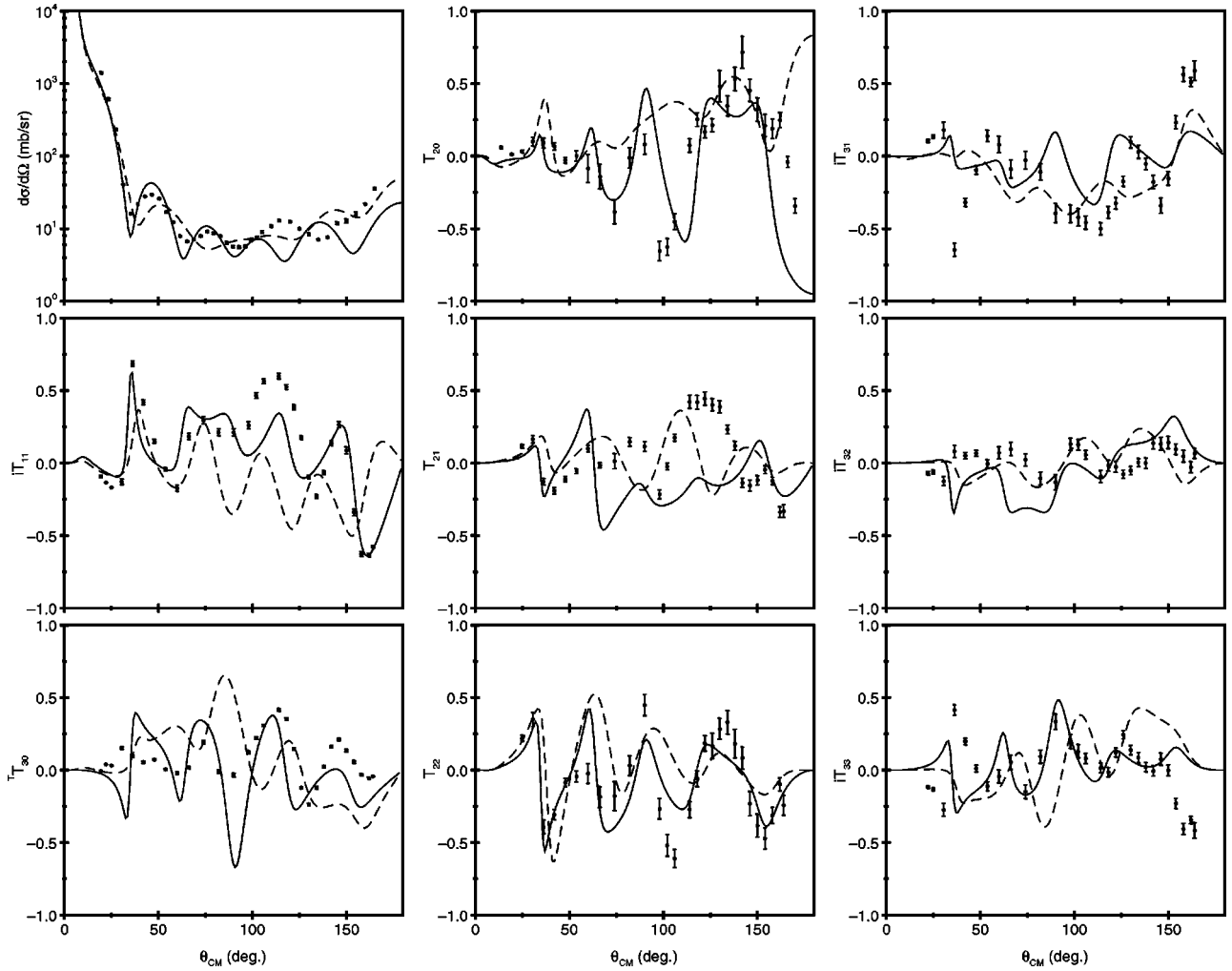


FIG. 4. Cross section and analyzing power angular distributions measured for the $^7$Li+$^4$He elastic scattering at a c.m. energy of 11.5 MeV. The full calculation using the optical model parameter set 3 in Table I is shown by the solid lines. The dashed line shows the full calculation without use of the third rank potential.

have because its importance was not recognized at that time, was added as it has been found to be important for $^7$Li scattering. The optical potential parameter values obtained for the 16.5 MeV c.m. scattering case were then changed as little as possible to fit the 11.5 MeV c.m. scattering. The optical potential parameter sets 2 and 4 in Table I are those finally used for the 16.5 and 11.5 MeV data, respectively. When these optical parameters were used in FRESCO, minus the tensor potentials, the values predicted were exactly the same. However, the tensor potential addition was not the same in both codes so the tensor potential depth was varied in FRESCO until the calculations were almost identical to those obtained with HERMES. The different values are given in brackets for parameter sets 2 and 4 in Table I. FRESCO does not allow a third rank potential, so none was used in the transfer calculations.

The $\alpha$-$t$ cluster spectroscopic factor for the $^7$Li ground state is close to unity. The code FRESCO with which the FRDWBA calculations were performed uses the spectroscopic amplitude (i.e., the square root of the spectroscopic factor $C^2S$) to set the magnitude of this transfer. Theoretical predictions give spectroscopic factors of 1.12 [28] and 1.19 [29], while values derived from past experiments are 0.94 $\pm$0.05 [30] and 1.03$\pm$0.10 [31].

The 16.5 MeV FRDWBA calculations using parameter set 2 in Table I and a spectroscopic amplitude of +1.0 are shown in Fig. 5. The solid lines show the transfer coherently added while the dashed lines do not include the transfer. The dotted line is the triton transfer cross section. Similar calculations for the 11.5 MeV data using parameter set 4 are shown in Fig. 6. Both negative and positive spectroscopic amplitudes were tried and no difference in the results was observed. The main goal here was not to fit the analyzing powers but to fit the cross section inner angles ($\theta_{\text{c.m.}} \leqslant 120°$) with the optical model parameters, and have the back angle cross section magnitude enhanced by the transfer. The analyzing powers generated by the optical model were made to give a reasonable description of the data and then the effects caused by the transfer addition were studied. A spectroscopic factor of 0.81 was also used for the 16.5 MeV case and the magnitude of the generated cross section at the far back angles was lower and closer to the data, when com-

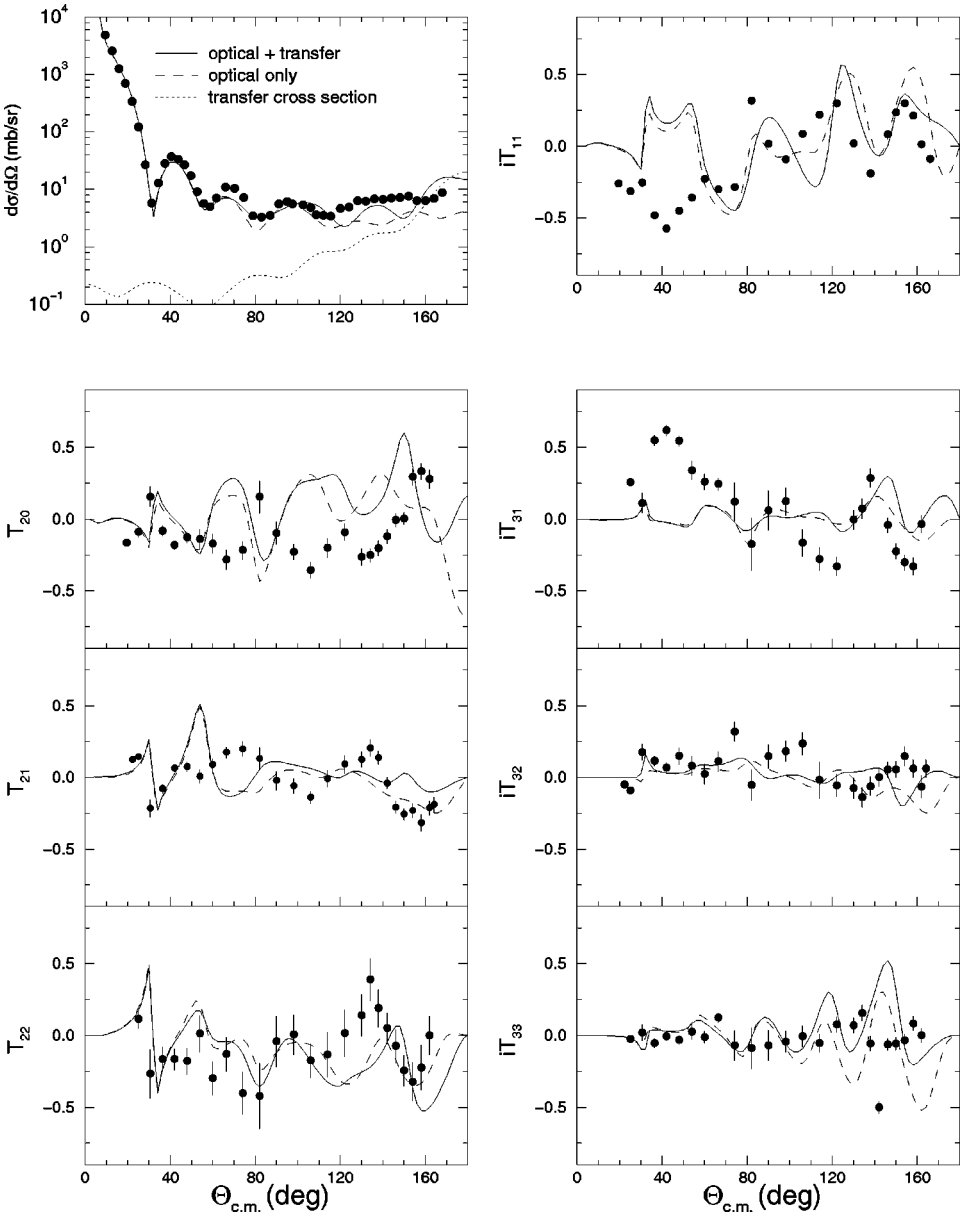


FIG. 5. Data are the same as in Fig. 3. The solid lines show the calculation using the parameter set 2 in Table I with the triton transfer included. The dashed lines show the calculation without the transfer added. The dotted line shows the transfer cross section.

pared to the fit with a spectroscopic factor of 1.0. However, the analyzing powers changed by only a negligible amount. A spectroscopic factor of 1.44 was used for the lower 11.5 MeV data for which the generated far back angle cross section were closer to the data. Here the analyzing powers also changed only slightly.

Both cases are quite similar, but at 11.5 MeV c.m. the transfer is more important. This result is also seen in the data, which shows a larger back angle cross section rise for the 11.5 MeV data. In both cases the optical model cross section, which concentrated on the forward angles, falls well short of the magnitude of the back angle data cross section. For the 16.5 MeV case the optical model gives a magnitude which is only 40% the size of the cross section data at back angles, while in the 11.5 MeV case it is only 25% the size. The cross section for the optical model levels out at back angles and misses the rise in the data. The transfer accounts for about 75% of the back angle cross section contributions in the 11.5 MeV case, and in the 16.5 MeV case it is lower but still accounts for 60%. In both cases the $iT_{11}$ generated is altered somewhat in magnitude at the back angles by the addition of the transfer, and the fit is actually improved for the 16.5 MeV case. The fit for the second rank analyzing powers at back angles does not change significantly but is somewhat poorer with the addition of the transfer, except for $T_{20}$ of the 16.5 MeV c.m. data. There are sign changes in the oscillations of $iT_{31}$ and $iT_{32}$ generated for the 16.5 MeV case with the addition of transfer, which lead to better fits. The third rank analyzing powers do not change much and are not really better fit with the addition of the triton transfer in the calculations.

In summary, the addition of a triton transfer contribution is needed and raises the back angle cross section generated by the optical model calculations to fit the data. The contribution is more important to the 11.5 MeV cross section than to the 16.5 MeV cross section. The odd rank analyzing

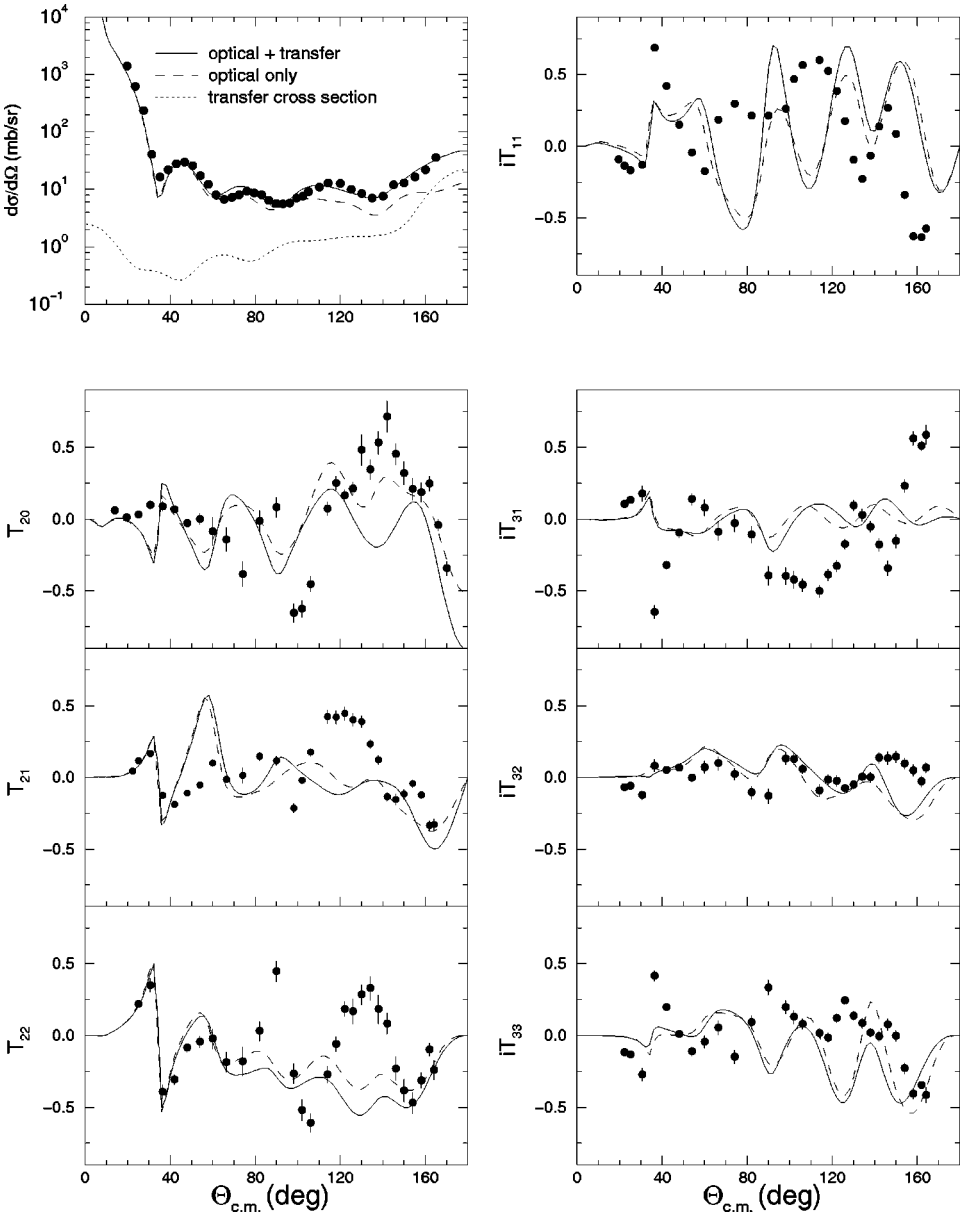


FIG. 6. Same as in Fig. 5 but for the 11.5 MeV c.m. data and using the parameter set 4 in Table I.

power fits are not changed much but are possibly improved by the transfer addition. The description of the second rank analyzing powers is also not changed much but is somewhat poorer with the addition of the transfer. In conclusion, triton transfer is present and contributes significantly to the back angle cross section, but does not have a large effect on the analyzing powers.

## IV. DISCUSSION

The present work presents the first complete set of third rank analyzing powers for the scattering of a spin 3/2 nucleus. The most striking result is that the third rank analyzing powers ${}^{T}T_{30}$, $iT_{31}$, $iT_{32}$, and $iT_{33}$ are large for both energies, and exhibit considerable structure. This is in contrast to the only other measurements of a third rank analyzing power, those of ${}^{T}T_{30}$ for 44 MeV ${}^{7}\mathrm{Li}+{}^{120}\mathrm{Sn}$ [7] and ${}^{7}\mathrm{Li}+{}^{26}\mathrm{Mg}$ [5], which were small and essentially structureless.

This difference in behavior could possibly be explained by the composite nature of ${}^{T}T_{30}$, which is given in terms of $iT_{31}$ and $iT_{33}$ by the following equation:

$$ {}^{T}T_{30} = -\left( \sqrt{\frac{3}{4}} iT_{31} + \sqrt{\frac{5}{4}} iT_{33} \right). \tag{20} $$

If $iT_{31}$ and $iT_{33}$ happen to be almost exactly out of phase they may cancel one another, leading to the small values of ${}^{T}T_{30}$ observed previously. If neither $iT_{31}$ nor $iT_{33}$ are well described by calculations, it might be expected that the calculated ${}^{T}T_{30}$ angular distribution would exhibit large oscillations that are not present in the data, as was found for the 44 MeV ${}^{7}\mathrm{Li}+{}^{26}\mathrm{Mg}$ system [5,8]. Even a small phase error in the description of $iT_{31}$ and/or $iT_{33}$ could lead to the large oscillations seen in the calculated ${}^{T}T_{30}$ angular distributions.

At present, this explanation must remain pure conjecture, as we do not have a full set of measured third rank analyzing

powers for the $^{7}$Li+$^{26}$Mg system. For the current data, we can see that $iT_{31}$ and $iT_{33}$ are *not* out of phase and thus do not cancel to give a small $^{T}T_{30}$. This illustrates the value of measuring a full set of third rank analyzing powers.

A comparison between previously measured $^{6}$Li+$^{4}$He and the present $^{7}$Li+$^{4}$He analyzing powers shows that differences between the structure of the two nuclei $^{6}$Li and $^{7}$Li are most apparent in the analyzing power $T_{21}$, with $T_{21}$ being large for $^{7}$Li and close to zero for $^{6}$Li. This implies that even for scattering energies where the nuclear interaction dominates, the $^{7}$Li nonspherical ground state shape is an important contributor to the scattering.

The optical model analysis of the present data set took two different approaches. One was to assume that the elastic scattering could be described by potential scattering only. The other analysis assumed that the large experimental cross section observed at backward angles was produced by triton exchange between the target and the projectile and that the forward angle cross section was produced by potential scattering. Both analyses show that a second rank tensor force is needed to produce the observed $T_{21}$ and $iT_{32}$ analyzing powers, which is consistent with the large ground state quadrupole moment of $^{7}$Li. They also show that the spin-orbit potential is small and the evidence for the presence of a third rank tensor potential of the form suggested by Mukhopadhyay *et al.* [9] is inconclusive. Its inclusion at 16.5 MeV leads to a degradation of the already far from good fit to the data. However, at 11.5 MeV the description of the data is considerably better when it is included. In fact, at 11.5 MeV the data are rather well described at angles $<100°$, the region in which the fit to the cross section is reasonably good, with the exception of $iT_{31}$ and $iT_{32}$ (the fit to $iT_{33}$, although better than for the other third rank analyzing powers, is still not as good as for the first and second ranks).

The failure to describe the forward angle third rank analyzing powers $iT_{31}$, $iT_{32}$, and $iT_{33}$ at either energy seems to indicate that the optical model potential form used in this work is incomplete. No calculations, even with completely unphysical parameters, were able to reproduce the small angle $iT_{31}$ data. However, owing to the large number of data points and adjustable parameters available we cannot claim to have exhausted the entire parameter space. In particular, we concentrated on a second derivative form for the third rank tensor potential, guided by the work of Mukhopadhyay *et al.* Tests with a third derivative form for this potential (suggested by a natural progression through the potential ranks of a first derivative spin-orbit potential and a second derivative second rank tensor potential) suggested that such a form would not lead to a significant improvement in the quality of the fits. The calculations that explicitly included triton transfer gave a better overall description of the data than did those that produced the back angle cross section by assuming its large magnitude was produced by channel coupling.

The present complete data set would enable scattering potentials to be obtained by the use of the iterative-perturbative $S$ matrix to potential inversion method which has been shown to be successful for the case of $^{6}$Li+$^{4}$He elastic scattering [32]. It is possible that such parity- and energy-dependent potentials would be able to establish definitely whether a third rank potential is required to describe the third rank analyzing powers and if so, what form it should take. However, at the present time this method can only be applied to scatterings with channel spin of 0, 1/2, or 1 and thus unfortunately cannot be used to examine this question.

## ACKNOWLEDGMENTS

The authors wish to acknowledge many enlightening discussions with Professor D. Robson. This work was supported by the State of Florida, the U.S. National Science Foundation, and the state Committee for Scientific Research of Poland (KBN) and CLG NATO grant.

[1] G. Tungate, R. Böttger, P. Egelhof, K.-H. Möbius, Z. Moroz, E. Steffens, W. Dreves, I. Koenig, and D. Fick, Phys. Lett. **98B**, 347 (1981).

[2] Z. Moroz, P. Zupranski, R. Böttger, P. Egelhof, K.-H. Möbius, G. Tungate, E. Steffens, W. Dreves, I. Koenig, and D. Fick, Nucl. Phys. **A381**, 294 (1982).

[3] K. Rusek, Z. Moroz, R. Čaplar, P. Egelhof, K.-H. Möbius, E. Steffens, I. Koenig, A. Weller, and D. Fick, Nucl. Phys. **A407**, 208 (1983).

[4] Z. Moroz, K. Rusek, P. Egelhof, S. Kossionides, K.-H. Möbius, G. Tungate, E. Steffens, G. Grawert, I. Koenig, and D. Fick, Nucl. Phys. **A417**, 498 (1984).

[5] W. Ott, R. Butsch, H. Jänsch, K.-H. Mobius, P. Paul, G. Tungate, E. Steffens, K. Rusek, Z. Moroz, I. M. Turkiewicz, K. Becker, K. Blatt, H. Leucker, and D. Fick, Nucl. Phys. **A489**, 329 (1988).

[6] K. Rusek, J. Giroux, H. Jänsch, H. Vogt, K. Becker, K. Blatt, A. Gerlach, W. Korsch, H. Leucker, W. Luck, H. Reich, H.-G. Völk, and D. Fick, Nucl. Phys. **A503**, 223 (1989).

[7] G. Tungate, D. Krämer, R. Butsch, O. Karban, K.-H. Möbius, W. Ott, P. Paul, A. Weller, E. Steffens, K. Becker, K. Blatt, D. Fick, B. Heck, H. Jänsch, H. Leucker, K. Rusek, Irena M. Turkiewicz, and Z. Moroz, J. Phys. G **12**, 1001 (1986).

[8] Y. Sakuragi, M. Yahiro, M. Kamimura, and M. Tanifugi, Nucl. Phys. **A480**, 361 (1988).

[9] D. Mukhopadhyay, G. Grawert, D. Fick, and Z. Moroz, Phys. Lett. **104B**, 361 (1981).

[10] P. V. Green, K. W. Kemper, P. L. Kerr, K. Mohajeri, E. G. Myers, D. Robson, K. Rusek, and I. J. Thompson, Phys. Rev. C **53**, 2862 (1996).

[11] G. M. Ter-Akopian, A. M. Rodin, A. S. Fomichev, S. I. Sidorchuk, S. V. Stepantsov, R. Wolski, M. L. Chelnokov, V. A. Gorshkov, A. Yu. Lavrentev, V. I. Zagrebaev, and Yu. Ts. Oganessian, Phys. Lett. B **426**, 251 (1998); R. Raabe, A. Andreev, D. Baye, W. Bradfield-Smith, T. Davinson, M. Gaelens, W. Galster, M. Huyse, J. McKenzie, A. Ninane, A. Piechaczek, A. C. Shotter, G. Vancraeynest, P. Van Duppen, and A. Wöhr, *ibid.* **458**, 1 (1999).

[12] G. Tungate and D. Fick, Lect. Notes Phys. **89**, 404 (1979); P. Zupranski, W. Dreves, P. Egelhof, K.-H. Möbius, E. Steffens, G. Tungate, and D. Fick, Phys. Lett. **91B**, 358 (1980).
[13] J. Gomez-Camacho and R. C. Johnson, J. Phys. G **12**, L235 (1986); **14**, 609 (1988).
[14] W. Ott, R. Butsch, H. Jänsch, G. Tungate, E. Steffens, K. Becker, K. Blatt, H. Leucker, D. Fick, J. Gomez-Camacho, and R. C. Johnson, J. Phys. G **14**, L7 (1988).
[15] E. G. Myers, A. J. Mendez, K. W. Kemper, P. L. Kerr, E. L. Reber, and B. G. Schmidt, Nucl. Instrum. Methods Phys. Res. A **334**, 271 (1993).
[16] H. G. Bingham, K. W. Kemper, and N. R. Fletcher, Nucl. Phys. **A175**, 374 (1971).
[17] P. D. Cathers, P. V. Green, E. E. Bartosz, K. W. Kemper, F. Maréchal, E. G. Myers, and B. G. Schmidt, Nucl. Instrum. Methods Phys. Res. A **457**, 509 (2001).
[18] E. E. Bartosz, P. D. Cathers, K. W. Kemper, F. Maréchal, D. Robson, G. Grawert, and K. Rusek, Phys. Lett. B **488**, 138 (2000).
[19] B. A. Robson, in *Proceedings of the 4th International Symposium on Polarization Phenomena in Nuclear Reactions*, Zürich, 1975, edited by W. Grüebler and V. König, Experientia Supplementum No. 25 (Birkhäuser Verlag, Basel, 1975), p. 423.
[20] D. E. Trcka, A. D. Frawley, K. W. Kemper, D. Robson, J. D. Fox, and E. G. Myers, Phys. Rev. C **41**, 2134 (1990).
[21] P. L. Kerr, K. W. Kemper, P. V. Green, K. Mohajeri, E. G. Myers, D. Robson, and B. G. Schmidt, Phys. Rev. C **52**, 1924 (1995).
[22] J. Cook, Comput. Phys. Commun. **31**, 363 (1984).
[23] J. Cook and R. J. Philpott, Nucl. Phys. **A385**, 157 (1982).
[24] J. Raynal, Phys. Lett. **7**, 281 (1963).
[25] M. Irshad and B. A. Robson, Nucl. Phys. **A218**, 504 (1974).
[26] I. J. Thompson, Comput. Phys. Rep. **7**, 167 (1988).
[27] A. Bisson and R. H. Davis, Phys. Rev. Lett. **22**, 542 (1969); R. A. Chatwin, J. S. Eck, D. Robson, and A. Richter, Phys. Rev. C **1**, 795 (1970).
[28] Yu. F. Smirnov and D. Chlebowska, Nucl. Phys. **26**, 306 (1961).
[29] O. F. Nemets, V. G. Neudatchin, A. T. Rudchik, Yu. F. Smirnov, and Yu. M. Tchuvilsky, *Nucleon Associations in Atomic Nuclei and Multi-Nucleon Transfer Reactions* (Ukranian Academy of Sciences, Institute for Nuclear Research, Kiev, 1988) [in Russian].
[30] P. G. Roos, N. S. Chant, A. A. Cowley, D. A. Goldberg, H. D. Holmgren, and R. Woody, Phys. Rev. C **15**, 69 (1977).
[31] N. Burtebaev, A. D. Duisebaev, B. A. Duisebaev, G. N. Ivanov, and S. B. Sakuta, Phys. At. Nucl. **59**, 29 (1996).
[32] R. S. Mackintosh, S. G. Cooper, and V. I. Kukulin, Nucl. Phys. **A645**, 399 (1999).